Earth and Planetary Science Letters 453 (2016) 260–266

Contents lists available at ScienceDirect

Earth and Planetary Science Letters

www.elsevier.com/locate/epsl

Magmatic oxygen fugacity estimated using zircon-melt partitioning of cerium

Duane J. Smythe [1], James M. Brenan [*,2]

Department of Earth Sciences, University of Toronto, Toronto, Canada

A R T I C L E   I N F O

Article history:
Received 7 January 2016
Received in revised form 4 August 2016
Accepted 8 August 2016
Available online 30 August 2016
Editor: M. Bickle

Keywords:
zircon
oxygen fugacity
magmas
cerium
Hadean

A B S T R A C T

Using a newly-calibrated relation for cerium redox equilibria in silicate melts (Smythe and Brenan, 2015), and an internally-consistent model for zircon-melt partitioning of Ce, we provide a method to estimate the prevailing redox conditions during crystallization of zircon-saturated magmas. With this approach, oxygen fugacities were calculated for samples from the Bishop tuff (USA), Toba tuff (Indonesia) and the Nain plutonic suite (Canada), which typically agree with independent estimates within one log unit or better. With the success of reproducing the fO_2 of well-constrained igneous systems, we have applied our Ce-in-zircon oxygen barometer to estimating the redox state of Earth's earliest magmas. Using the composition of the Jack Hills Hadean zircons, combined with estimates of their parental magma composition, we determined the fO_2 during zircon crystallization to be between FMQ -1.0 to $+2.5$ (where FMQ is the fayalite–magnetite–quartz buffer). Of the parental magmas considered, Archean tonalite–trondhjemite–granodiorite (TTG) compositions yield zircon-melt partitioning most similar to well-constrained modern suites (e.g., Sano et al., 2002). Although broadly consistent with previous redox estimates from the Jack Hills zircons, our results provide a more precise determination of fO_2, narrowing the range for Hadean parental magmas by more than 8 orders of magnitude. Results suggest that relatively oxidized magmatic source regions, similar in oxidation state to that of 3.5 Ga komatiite suites, existed by ~4.4 Ga.

1. Introduction

The mineral zircon incorporates a variety of trace elements during crystallization, including the rare-earth elements (REE), uranium, thorium, and titanium, which makes this phase particularly useful for tracing magma chemistry as well as for geochronometry and geothermometry (Hoskin and Schaltegger, 2003; Watson and Harrison, 2005). A nearly ubiquitous, but until recently underutilized, feature of terrestrial zircon (though generally lacking in lunar and meteoritic samples) is the anomalously high chondrite-normalized concentration of Ce relative to neighboring REEs. In most terrestrial magmas, Ce will exist in both 3+ and 4+ oxidation states (Trail et al., 2011, 2012; Burnham and Berry, 2012, 2014; Smythe and Brenan, 2015), so anomalous Ce concentrations in zircon result from the favored partitioning of Ce^{4+} relative to Ce^{3+} into the zircon structure; Ce^{4+} is isovalent with, and a close match in ionic radius to Zr^{4+} (Shannon, 1976). The change in Ce oxidation state in silicate melts can be expressed via the homogeneous reaction,

$$CeO_{3/2}^{melt} + \frac{1}{4}O_2^{melt} = CeO_2^{melt} \quad (1)$$

This implies that the relative proportions of Ce^{3+} ($CeO_{3/2}$) and Ce^{4+} (CeO_2) in a silicate melt will be a function of the oxygen fugacity (fO_2) of the system, and the magnitude of the resulting Ce anomaly in zircon will then be a record of the prevailing redox conditions during crystallization. In principle, it might be possible to measure the Ce^{4+}/Ce^{3+} in zircon directly as an indicator of magma oxidation state. However, alpha recoil events during radioactive decay of U and Th induce structural changes in zircon (Trachenko et al., 2002), which allow for post-crystallization changes in Ce^{4+}/Ce^{3+}, making this approach unreliable. Instead, because the sluggish diffusion rates of 3+ and 4+ cations in zircon (Cherniak et al., 1997a, 1997b) prevent modification of absolute Ce concentrations, Ce anomalies produced during crystal growth potentially constitute a robust record of magma redox state.

Recently, Trail et al. (2011, 2012) provided an experimental calibration that relates the magnitude of the Ce anomaly in zircon, termed $(Ce/Ce^*)_D$ (in which Ce^* is the estimated value for

* Corresponding author.
E-mail address: jbrenan@dal.ca (J.M. Brenan).
[1] Present address: Department of Earth Sciences, Oxford University, Oxford, United Kingdom.
[2] Present address: Department of Earth Sciences, Dalhousie University, Halifax, Canada.

http://dx.doi.org/10.1016/j.epsl.2016.08.013

$D^{zircon/melt}_{Ce^{3+}}$), to fO_2 and temperature. Values of $(Ce/Ce^*)_D$ can be calculated from natural samples from knowledge of the bulk partition coefficient for Ce, combined with the estimated value for $D^{zircon/melt}_{Ce^{3+}}$ as interpolated from partition coefficients for the neighboring light REEs (LREEs), La and Pr. This approach is a valuable first step in exploiting the Ce anomaly as a redox sensor, but seems to yield relatively imprecise estimates for magma fO_2 (possible reasons for this are discussed later). As an alternative, we have taken the approach of Ballard et al. (2002), in which the concentration of Ce in zircon and melt, along with values of $D^{zircon/melt}_{Ce^{3+}}$ and $D^{zircon/melt}_{Ce^{4+}}$ are related to the mole fractions of Ce^{4+}($x^{melt}_{Ce^{4+}}$) and Ce^{3+} ($x^{melt}_{Ce^{3+}}$) in the melt by the equality:

$$\left[\frac{x^{melt}_{Ce^{4+}}}{x^{melt}_{Ce^{3+}}}\right] = \left[\frac{\sum Ce_{zircon} - (\sum Ce_{melt} * D^{zircon/melt}_{Ce^{3+}})}{(\sum Ce_{melt} * D^{zircon/melt}_{Ce^{4+}}) - \sum Ce_{zircon}}\right] * 1.04877 \tag{2}$$

where ΣCe is the total concentration of Ce in zircon or melt, and the constant 1.04877 is the mole to wt% conversion factor. Using results from our previous work on the redox behavior of Ce in silicate melts (Smythe and Brenan, 2015), the relative proportions of Ce^{4+} and Ce^{3+} can be related to melt fO_2 through the equation:

$$\ln\left[\frac{x^{melt}_{Ce^{4+}}}{x^{melt}_{Ce^{3+}}}\right] = \frac{1}{4}\ln fO_2 + \frac{13136(\pm 591)}{T} - 2.064(\pm 0.011)\frac{\mathrm{NBO}}{\mathrm{T}} - 8.878(\pm 0.112)\cdot xH_2O - 8.955(\pm 0.091) \tag{3}$$

where T is in Kelvin and can be determined using the Ti-in-zircon thermometer (Ferry and Watson, 2007), NBO/T is the proportion of non-bridging oxygens to tetrahedrally coordinated cations (Virgo et al., 1980) calculated on an anhydrous basis (assuming all ferrous iron), and xH_2O is the mole fraction of water dissolved in the melt. Zircon/melt partition coefficients for Ce^{3+} ($D^{zircon/melt}_{Ce^{3+}}$) and Ce^{4+} ($D^{zircon/melt}_{Ce^{4+}}$) can be calculated for individual zircon-melt pairs using the lattice strain model of Blundy and Wood (1994), and are constrained by the partition coefficients for the other REEs as well as Hf, Th, and U (as described below). In this communication, we demonstrate the accuracy of this new oxygen barometer through application to three zircon-saturated igneous suites whose redox state has been determined by independent methods. We then show how the method can be used to estimate the fO_2 during crystallization of magmas formed within 500 million years of terrestrial accretion, as represented by the Hadean-aged Jack Hills zircons.

2. Samples investigated

Samples investigated in this study were taken from three different localities for which fO_2 has been estimated previously, namely: the Bishop tuff (California), Toba tuff (Indonesia), and Umiakovik pluton (Nain plutonic suite, Labrador). Eruption of Bishop tuff occurred at 760 ka and the unit consists of several packages of fall deposits and ignimbrite. Samples of Bishop tuff were obtained from the Ig2E unit as defined by Wilson and Hildreth (1997), and consist of high-silica rhyolite pumices containing <5% crystal fragments, primarily of quartz, in a glassy matrix. Fourier transform infrared (FTIR) spectroscopy of melt inclusions in quartz have determined the H_2O content of the pre-eruptive magma to be between 5.1 and 6.8 wt% (Anderson et al., 1989; Wallace et al., 1999). Oxygen fugacity and temperature for Bishop tuff samples, calculated from Fe–Ti-oxide thermobarometry, range from ΔFMQ of +0.5 to +2.0 and ∼700 to 840 °C (Hildreth and Wilson, 2007). The Toba tuff sample is a potassic high-silica rhyolitic welded tuff that erupted at 74 ka, belonging to the youngest

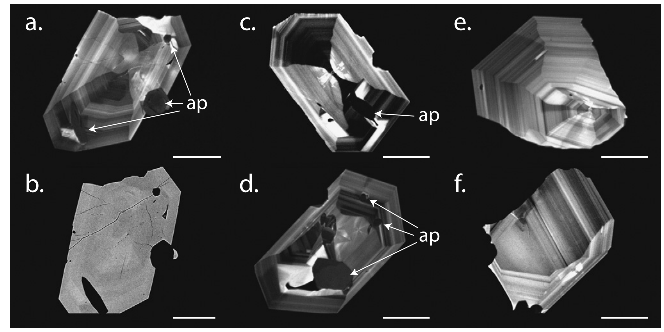

Fig. 1. Representative zircon textures from the Bishop tuff. Images a) and b) are CL and BSE images, respectively, of 12-BT2-9, c) through f) are CL images of 12-BT-1, 12-BT2-3, 12-BT2-4 5, 12-BT2-2, respectively. Prominent sector and oscillatory zoning are present in all zircons. Samples in a) and d) contain partially resorbed cores which appear bright in CL, and dark in BSE. Apatite (ap) inclusions are common and are found in most crystals. Scale bars = 50 μm.

unit in the Toba volcanic package (YTT as defined by Chesner, 1998). The sample is primarily composed of ∼25% crystal fragments (consisting of quartz, plagioclase, sanidine, and biotite) in a partially devitrified glass matrix. Oxygen fugacity and temperature for Toba tuff samples, also calculated from Fe–Ti-oxide thermobarometry, yielded ΔFMQ of 0 to +1.5 and 680 to 850 °C (Chesner, 1998). Melt inclusions analyzed by FTIR spectroscopy constrain the pre-eruptive H_2O content of the Toba tuff to between 4.0 and 5.5 wt%. For the cases of Bishop tuff and Toba tuff, we adopt the higher value within each range of H_2O content for the calculations. The sample from Umiakovik pluton (Geological Survey of Canada sample number EC87-86) is a pyroxene-bearing quartz monzodiorite that intruded Archean and Proterozoic gneisses 1311–1320 Ma (Emslie and Loveridge, 1992). The fO_2 and temperature of crystallization for the Umiakovik pluton, estimated by the intersection of isopleths defined by the hematite content of ilmenite and the ferric–ferrous ratio of biotite, range from ΔFMQ of −1 to −4 and 710 to 840 °C. The water content of the Umiakovik pluton magma is somewhat less straightforward to estimate, as primary melt inclusions have not been documented. Instead, the fH_2O has been calculated, from biotite-melt phase relations, to be ∼250 bars (Emslie and Stirling, 1993), equivalent to ∼4.5 wt% H_2O.

Zircons obtained from Bishop tuff are clear, and generally have a prismatic crystal habit, ranging in size from ∼50 to 200 μm. Inclusions of apatite were found in nearly all of the Bishop tuff zircons. Back-scattered electron (BSE) and cathodoluminescence (CL) images show relatively simple chemical zonation with sector zoning superimposed on oscillatory growth zoning (Fig. 1). Approximately half of the zircons from Bishop tuff contain cores with a relatively high CL response. Zircons from Toba tuff are clear, highly elongate prisms up to 300 μm in length with abundant apatite and melt inclusions (Fig. 2). From BSE and CL imaging, the Toba tuff zircons appear to have a relatively complex growth history, showing in some cases multiple episodes of growth and resorption. The outer domains in all Toba tuff zircons have oscillatory zoning occasionally with faint sector zoning. Umiakovik pluton zircons are typically 100 to 500 μm in size with tabular to prismatic morphologies (Fig. 3). Grains vary from colorless to pale brown and generally lack mineral inclusions. Imaging shows broad and oscillatory zoning in the outer domains of most samples, cored by regions with convolute zoning or lacking any internal structure suggesting recrystallization. Chemical analyses of all zircons were restricted to pristine regions with oscillatory growth zoning. Central domains interpreted to be regions of early growth were avoided.

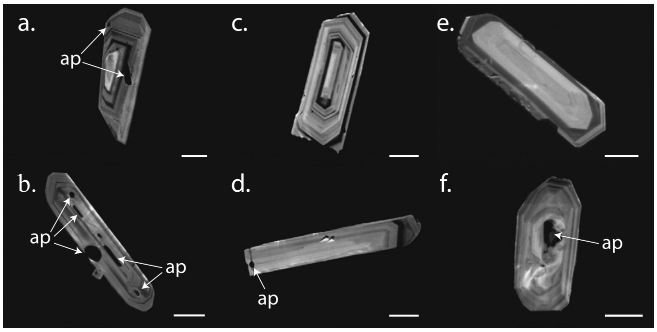

Fig. 2. Cathodoluminescence images of typical zircons from the Toba tuff. The outer regions of all samples show oscillatory zoning. Some grains contain cores, which may be either euhedral (e) or partially resorbed (a). Apatite inclusions are common and occur in almost all grains. Images shown are of samples TT-49 (a), TT-27 (b), TT-40 (c), TT-55 (d), TT-23 (e) and TT-36 (f). Scale bars = 50 μm.

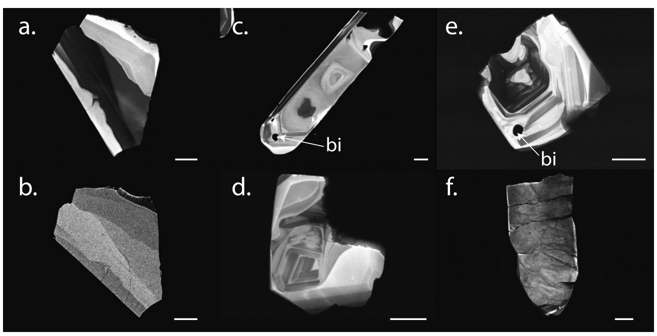

Fig. 3. Representative textures of zircons from Umiakovik pluton. Images a) and b) are Cl and BSE images of samples 12-UB-Z11, c) through f) are CL images of samples 12-UB-Z48, 12-UB-Z6, 12-UB-Z18 and 12-UB-Z4, respectively. Zircons from this suite typically have outer domains with either broad (a, b, and d) or oscillatory zoning (c and e). Inner domains often contain xenocrystic cores (c), and tend to have convolute zoning (e). In some cases zircons appear to be partially, or entirely recrystallized (f). Mineral inclusions, other than biotite (bi), are rare in Umiakovik pluton zircons. Scale bars = 50 μm.

3. Analytical methods

The whole-rock analysis of the Umiakovik pluton sample was done on a powdered aliquot obtained from the Geological Survey of Canada using solution ICP-MS at Activation Laboratories in Ancaster, Ontario, Canada. Accuracy and precision of trace element analyses are within 10 and 4% of the measured values, respectively, with detection limits of 0.01 ppm or better. Major and trace element analyses of zircons and natural glass were done in the Department of Earth Sciences, University of Toronto. Major element compositions were determined using a Cameca SX50 electron microprobe. Analyses of glasses were done at 15 kV using a 20 μm defocused beam and 5 nA beam current. Alkali elements were measured at the beginning of the acquisition, so as to minimize their migration under the electron beam. Standards employed were natural basaltic glass (Mg, Ca, Mn, Fe), obsidian (Si, Al), albite glass (Na), sanidine (K), TiO_2 (Ti), and $CePO_4$ (P). Major element analysis of zircon was done using a 20 kV accelerating voltage, 50 nA beam current and 1 μm beam size. Standards used include synthetic zircon (Zr, Si), hafnon (Hf), and YPO_4 (Y, P). Raw count rates were converted to element concentrations using the ZAF correction routine.

The trace element content of the glasses from Bishop tuff and Toba tuff, and zircons from all samples, were determined by LA-ICP-MS. The system at the University of Toronto employs a Thermo Elemental (VG) PlasmaQuad PQ ExCell ICP-MS coupled to a NuWave UP-213 laser and ablation cell. NIST 610 glass was used to quantify trace element concentrations using the following isotopes: ^{31}P, ^{44}Ca, ^{47}Ti (in glass), ^{49}Ti (in zircon), ^{89}Y, ^{139}La, ^{140}Ce, ^{141}Pr, ^{146}Nd, ^{147}Sm, ^{153}Eu, ^{157}Gd, ^{159}Tb, ^{163}Dy, ^{165}Ho, ^{166}Er, ^{169}Tm, ^{172}Yb, ^{175}Lu, ^{178}Hf, ^{232}Th, and ^{238}U. ^{44}Ca and ^{180}Hf were used to monitor ablation yields in glass and zircon, respectively (^{178}Hf was also measured in zircon to check for potential interferences from REE-oxides). On-peak dwell times of 10 ms were used for all elements, except La and Pr in zircon, for which counts were measured for 30 ms, due to low concentrations. We used ^{49}Ti to quantify Ti abundances in zircon to avoid the doubly charged ^{94}Zr species, which causes a significant interference on mass 47. Glass and zircon analyses were done using 50 and 20 μm spots, respectively, with a laser repetition rate of 10 Hz. Beam fluence was adjusted to optimize aerosol production. During zircon analysis, the signals from ^{27}Al and ^{44}Ca were monitored to screen for contamination by other phases. Major and trace element analyses of glass and zircon, including limits of detection, are provided in Supplemental Tables S1 and S2, respectively.

Measurements of glass compositions are in close agreement with previous determinations of melt inclusions trapped in quartz and sanidine (Wallace et al., 1999; Anderson et al., 2000; Chesner and Luhr, 2010), although the glass from Toba tuff samples contained ∼6.7 wt% potassium, which is somewhat higher than values of ∼5.2 wt% quoted for the same unit in earlier studies (Chesner and Luhr, 2010; Table S1). For the Bishop tuff and Toba tuff samples, rather than use the composition of the glass hosting the zircons, we chose to employ the major and trace element composition of melt inclusions, so as to most closely represent the composition of the zircon-forming magma (Table S1). For the Bishop tuff melt, the average composition of five melt inclusions from Anderson et al. (2000) from samples within the Ig2E or equivalent unit were selected (11A-F1, 11B-F1, 15-F1-1, 15-F1-2, 133A-7-1) and the Toba melt composition is from Chesner and Luhr (2010; their sample 5B3-3 MI).

4. Lattice strain constraints on Ce partitioning

Using the estimations of melt composition and the measured trace element concentrations in zircon, values of $D_{\mathrm{Ce}}^{zircon/melt}$ can be calculated. Estimates for $D_{\mathrm{Ce}^{3+}}^{zircon/melt}$ and $D_{\mathrm{Ce}^{4+}}^{zircon/melt}$ can be made after the method of Ballard et al. (2002). In this approach, partition coefficients for the trivalent REEs and the quadrivalent series Hf, Th, and U are used to constrain $D_{\mathrm{Ce}^{3+}}^{zircon/melt}$ and $D_{\mathrm{Ce}^{4+}}^{zircon/melt}$, respectively. Blundy and Wood (1994) showed that the mineral melt partition coefficient for a cation i can be related to the lattice strain energy created by substituting a cation whose ionic radius (r_i) differs from the optimal value for that site (r_0). They provide the expression,

$$D_i = D_0 \times \exp\left[\frac{4\pi E N_A[\frac{r_0}{2}(r_i - r_0)^2 + \frac{1}{3}(r_i - r_0)^3]}{RT}\right] \quad (4)$$

where D_0 is the 'strain compensated partition coefficient', E is the Young's Modulus, N_A is Avogadro's number, R is the gas constant, and T is the temperature in degrees K. Rearranging Equation (4) and taking the logarithm of both sides, yields the relation:

$$\ln D_i = \ln D_0 - \frac{4\pi E N_A}{RT}\left(\frac{r_i}{3} + \frac{r_0}{6}\right)(r_i - r_0)^2 \quad (5)$$

Plotting $\ln D_i$ against the term $(r_i/3 + r_0/6)(r_i - r_0)^2$ therefore yields a linear relation for an isovalent series of cations. With knowledge of the ionic radii of Ce^{3+} and Ce^{4+}, partition coefficients for these species can be determined by interpolation. Since Ce will be a mixture of Ce^{3+} and Ce^{4+}, the value of $D_{\mathrm{Ce}}^{zircon/melt}$ will lie between these two partition coefficient end-members, and

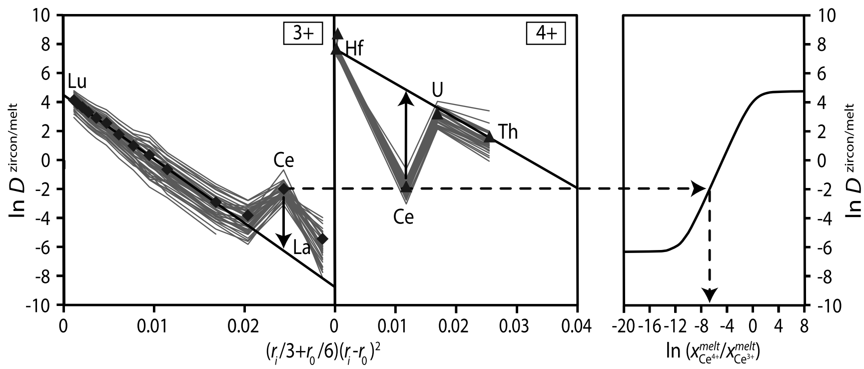

Fig. 4. Graphical representation of the procedure used to estimate fO_2 from a combination of zircon-melt partitioning of Ce, and the relation between melt $x^{melt}_{Ce^{4+}}/x^{melt}_{Ce^{3+}}$ vs fO_2 provided in Smythe and Brenan (2015). In this example, values of $\ln D_i^{zircon/melt}$ were calculated from individual zircon and glass analyses from samples of the Toba tuff. Average values are shown as points, whereas lines connect results from individual analyses. The partition coefficients for 3+ (left) and 4+ (center) cations display linear arrays when plotted as a function of the Blundy and Wood (1994) lattice strain parameter, $(r_i/3+r_0/6)(r_i-r_0)^2$. The interpolated values of $D^{zircon/melt}_{Ce^{4+}}$ and $D^{zircon/melt}_{Ce^{3+}}$ based on their ionic radii (Shannon, 1976) are used to define the upper and lower asymptotes for the change in $D^{zircon/melt}_{Ce}$ with $x^{melt}_{Ce^{4+}}/x^{melt}_{Ce^{3+}}$. The measured $D^{zircon/melt}_{Ce}$ lies between these limits and can then be used to calculate a value of $x^{melt}_{Ce^{4+}}/x^{melt}_{Ce^{3+}}$, and hence fO_2. Adapted from Ballard et al. (2002).

through combination of Equations (3) and (5) can be used to determine the fO_2 during crystallization. A graphical example of this procedure for estimating the fO_2 of the Toba tuff samples is portrayed in Fig. 4.

Ionic radii for the REEs, Hf, U and Th were taken from the compilation of Shannon (1976). In practice, we excluded the LREEs, La and Pr, in the fitting procedure for 3+ cations as these elements are present at very low levels in natural zircons, and concentrations are highly susceptible to contamination by accessory mineral inclusions. Eu was also excluded, as it can exist as both Eu^{2+} and Eu^{3+} species, the former being sensitive to plagioclase fractionation. Values of r_0 used for 3+ and 4+ cations were 0.93 Å (determined by regression) and 0.83 Å (8-fold coordinated Hf), respectively.

Temperatures were calculated using the Ti content of zircon, using the expression (Ferry and Watson, 2007):

$$\log(\mathrm{Ti}_{zircon}) = (5.711 \pm 0.072) - \frac{4800 \pm 86}{T} - \log a\mathrm{SiO_2} + \log a\mathrm{TiO_2} \quad (6)$$

where Ti_{zircon} is the concentration of Ti in zircon in ppm, T is temperature degrees K, and a_i is the ratio of the concentration of component i in the melt over the concentration of component i in the melt at saturation. For the samples under investigation, $a\mathrm{SiO_2}$ can be assumed to be unity, as all systems reached quartz saturation, and $a\mathrm{TiO_2}$ was calculated using the TiO_2 solubility model of Hayden and Watson (2007).

Propagation of error through the fO_2 calculation, including the error in Ce^{3+}/Ce^{4+} in the melt (equation (3)), Ti crystallization temperatures (equation (6)), analytical errors in the calculated NBO/T as well as xH_2O, yields an estimated uncertainty in the accuracy of ~1 log unit. We have provided an Excel spreadsheet in the electronic appendix for the user to calculate magma fO_2 by the above-described method, with input parameters as defined above.

5. Comparison to independent estimates of magma fO_2 and temperature

Oxygen fugacity and temperature calculated for the Bishop tuff, Toba tuff and Umiakovik pluton suites are portrayed in Fig. 5. As is typical for volcanic suites undergoing prolonged cooling and eruption, the data for the Bishop tuff and Toba tuff suites describe linear arrays in fO_2–T space, roughly parallel to the FMQ buffer (Carmichael, 1991). The arrays for the Bishop tuff and Toba

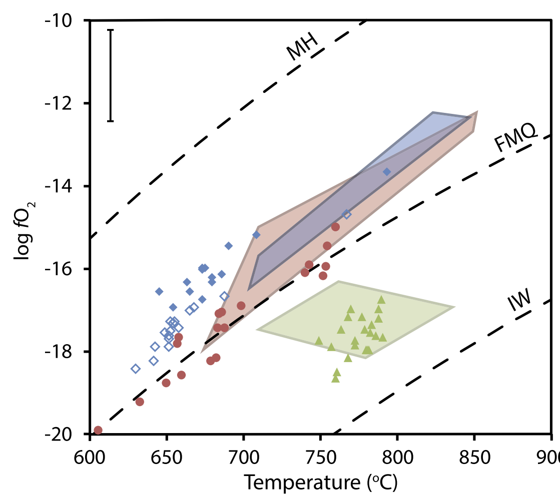

Fig. 5. Values of $\log fO_2$ calculated using the Ce-in-zircon oxygen barometer presented in this study as a function of temperature for zircons from the Bishop tuff (solid blue diamonds this study, hollow blue diamonds from Reid et al., 2011), Toba tuff (red circles), and Umiakovik pluton (green triangles) compared to independent estimates (equivalently-colored fields). Temperatures were calculated using zircon Ti contents and the calibration of Ferry and Watson (2007). Independent estimates of fO_2 and T for the Bishop and Toba volcanic samples are derived from Fe–Ti oxide (Chesner, 1998; Hildreth and Wilson, 2007). Values for the Umiakovik pluton were estimated by the intersection of isopleths defined by the hematite content of ilmenite and the ferric–ferrous ratio of biotite (Emslie and Stirling, 1993). Typical error in calculated fO_2 is shown in the upper left corner (approximately $+/-1$ log unit). The dashed black curves correspond to the variation in fO_2 with T along the FMQ buffer, calculated from O'Neill (1987), the magnetite–hematite (MH) and iron–wustite (IW) buffers calculated from O'Neill (1988). (For interpretation of the references to color in this figure, the reader is referred to the web version of this article.)

tuff suites defined by thermobarometry involving either zircon or the Fe–Ti oxides overlap at higher temperature, and most of the zircon-based fO_2 estimates extend to lower T, but parallel to the buffer curves. The higher degree of scatter for the arrays defined by zircon thermobarometry may not be too surprising, given possible variations in melt chemistry and temperature, which may occur during protracted zircon growth in the crust (e.g., Claiborne et al., 2010). Indeed, there is evidence for compositional zoning in the pre-eruptive magmas of both the Bishop tuff and Toba tuff systems (Chesner, 1998; Hildreth and Wilson, 2007). In our calculations, we assume that melt inclusion compositions are representative of the magma from which all the zircons from the Bishop tuff and Toba tuff suites formed, whereas this only strictly applies to the zircon containing that inclusion. As for the Umiakovik pluton, calculated zircon crystallization temperatures and fO_2s directly overlap with those determined from biotite-oxide equilibria, indicating that zircon likely formed simultaneously.

6. Estimation of the redox state of Hadean magmas

Detrital zircon grains occurring in ca. 3 Ga conglomerates from Jack Hills in the Narryer Gneiss Complex, Western Australia, have U–Pb ages ranging from 3.0 Ga to as old as 4.404 ± 0.008 Ga (Wilde et al., 2001), the oldest of which crystallized within 150 Ma of terrestrial accretion. The REE patterns of the Hadean grains have been shown to fall into one of two categories, a LREE depleted group (*type-1*), taken to represent pristine magmatic zircon, and a LREE enriched group (*type-2*), interpreted to be hydrothermally altered (Hoskin, 2005). Application of the model presented here to estimate the fO_2 of the magma parental to the *type-1* Hadean zircons from Jack Hills is a challenge, as care must be made in the assumptions regarding the major and trace element chemistry, as well as water content, of the Hadean zircon-forming melt. As outlined by Watson and Harrison (1983), conditions that will promote zircon crystallization in magmatic systems are a general increase in melt SiO_2 content, as well as a decrease in temperature. Consistent with this notion are constraints from both oxygen isotopic data (Wilde et al., 2001), mineral inclusions (Maas et al., 1992), and Ti thermometry (Watson and Harrison, 2005; Carley et al., 2014) suggesting that the Hadean Jack Hills zircons crystallized from relatively low temperature, hydrous, felsic magmas.

What is more difficult to constrain is the relative trace element abundances of the parent melt from which the Jack Hills zircons crystallized. One approach is to simply use published experimental or empirical values of zircon-melt partitioning. However, results of experimental investigations of zircon-melt partitioning have shown that the uptake of REE with partition coefficients that differ significantly from unity can be over- or under-estimated (depending if $D_i^{zircon/melt} < 1$ or >1, respectively) due to slow diffusion in the melt phase (Luo and Ayers, 2009). Studies on natural systems have yielded a wide range of zircon/melt partition coefficients (Fujimaki, 1986; Hinton and Upton, 1991; Nagasawa, 1970; Sano et al., 2002; Thomas et al., 2002), with values for the REEs differing by up to four orders of magnitude. Although it is possible that some of this variation is the result of contamination by REE-rich phases during zircon analysis (particularly the LREEs), other factors, such as the availability of charge compensating ions (e.g., phosphorous), temperature, or composition of the crystallization environment, are also likely to play an important role. Despite this shortcoming, values for $D_i^{zircon/melt}$ determined by Sano et al. (2002) seem to provide an accurate estimate of zircon-hosted melt compositions (Hanchar and van Westrenen, 2007; Luo and Ayers, 2009) for the 3+ REEs. In this case, we use the partition coefficients measured by Sano et al. (2002) as a basis for comparison. We have calculated values for $D_i^{zircon/melt}$ dividing the trace element concentrations of the Jackhills zircons by the trace element concentration of three different types of potential parental magma compositions: pyrolite (i.e., equivalent to unmelted upper mantle; McDonough and Sun, 1995), bulk continental crust (Rudnick and Gao, 2003), and Archean tonalite–trondhjemite–granodiorite (TTG, Martin, 1995). Comparison of partition coefficients calculated for these different melt reservoirs, with values measured by Sano et al. (2002), show the greatest degree of overlap with the Archean TTG as the parent melt (Fig. 6). These values, combined with measured concentrations in Hadean zircons, have been used to estimate magma fO_2. In this case, we have restricted our zircon dataset to spot analyses

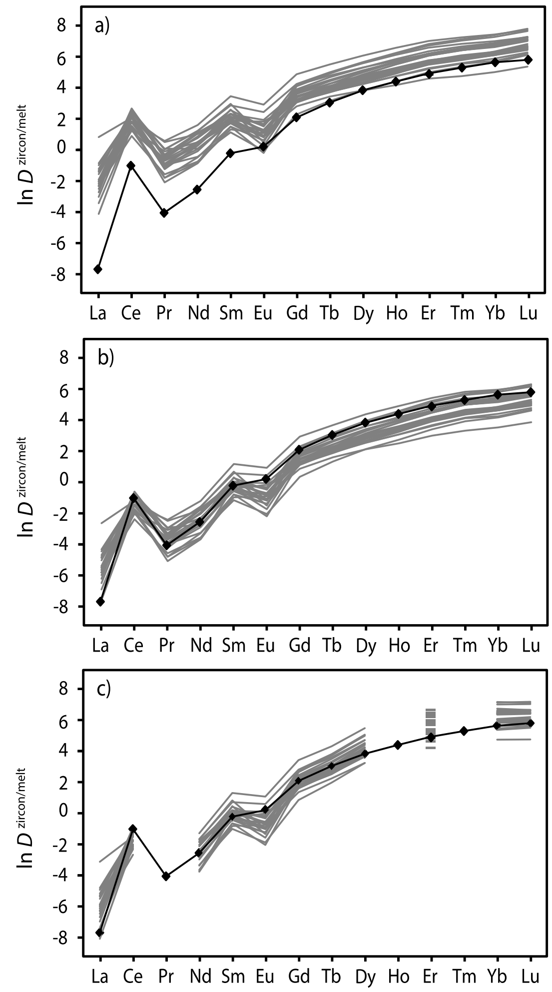

Fig. 6. Plot of log $D_i^{zircon/melt}$ calculated for the Jack Hills zircons assuming different parent melt trace element compositions (gray lines). Also plotted are partition coefficients from Sano et al. (2002, black diamonds). A) pyrolite (McDonough and Sun, 1995), B) bulk continental crust (Rudnick and Gao, 2003), C) Archean TTG (Martin, 1995).

of oscillatory zone domains with magmatic REE patterns, for which U–Pb age, oxygen isotopic composition, and crystallization temperature have been determined, totaling 23 analyses (Cavosie et al., 2006; Fu et al., 2008). This allows for calculation of $D_i^{zircon/melt}$ values for 3+ and 4+ cations, and from the method outlined above determination of $x_{Ce^{4+}}^{melt}/x_{Ce^{3+}}^{melt}$. This is not to say that the Hadean melts from which these zircons crystallized are necessarily the same as Archean TTG, only that the relative trace element abundances of interest here are similar.

By estimating the anhydrous NBO/T values for felsic magmas (e.g., broadly dacite–rhyolite) to range between 0.01 and 0.20, and assuming water contents of typical modern felsic melts (2.5 to 6.5 wt%) we approximate the likely range for the compositional terms in Equation (3) (shown by the horizontal bar in Fig. 7). Within one standard deviation of the calculated values of $x_{Ce^{4+}}^{melt}/x_{Ce^{3+}}^{melt}$ for a TTG composition (vertical bar in Fig. 7), we estimate the possible range of fO_2 for the Jack Hills zircon to lie between FMQ −1.0 to +2.5. As shown in Fig. 7, estimates of fO_2 are quite sensitive to changes in H_2O and NBO/T. If a completely anhydrous composition was assumed, the resulting fO_2 would be 2.5 log units lower than for the same melt with ∼5 wt% H_2O. On the other hand, if a basaltic composition was used in place of a granitic composition the resulting change in the NBO/T term would increase the calculated fO_2 by ∼3 log units. As mentioned earlier,

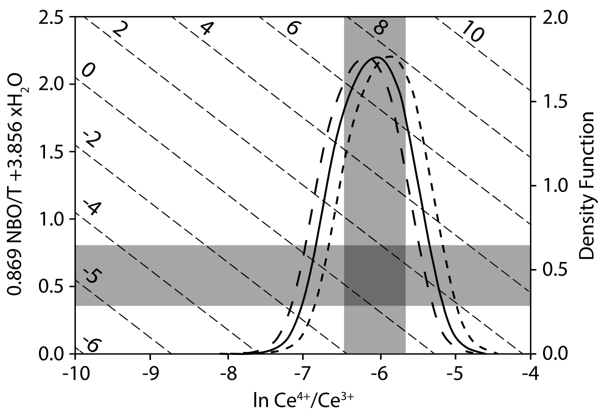

Fig. 7. Diagram depicting the compositional terms from Equation (3) as a function of the calculated values for $\ln x^{melt}_{Ce^{4+}}/x^{melt}_{Ce^{3+}}$ for analyses of the >4.0 Ga Jack Hills zircons. Analyses selected were from oscillatory zone regions, with magmatic REE patterns, for which oxygen isotopic composition and crystallization temperature had been determined. The probability density functions for calculated $\log x^{melt}_{Ce^{4+}}/x^{melt}_{Ce^{3+}}$ are plotted on the right hand vertical axis, corresponding to different parent melt trace element concentrations (pyrolite = coarse dashed curve; bulk continental crust = fine dashed curve; Archean TTG = solid curve). Diagonal dashed lines are fO_2 isopleths, labeled according to the log fO_2 relative to the FMQ buffer at 750 °C. The horizontal gray bar corresponds to the likely range in the melt composition parameter for zircon crystallizing melts. The vertical gray bar is one standard deviation in the calculated values of $x^{melt}_{Ce^{4+}}/x^{melt}_{Ce^{3+}}$ determined assuming an Archean TTG parental magma. The box defined by the intersection of the two bars denotes a range in fO_2 estimates for Hadean zircons of approximately FMQ −1.0 to +2.5.

melts of this nature do not typically saturate in zircon, nor appear to pertain to the parent melts of the Jack Hills zircons, therefore, these are not included in the estimated compositional range.

These results, although broadly consistent with previous redox estimates from these zircons (Trail et al., 2011), are on average slightly more oxidizing. Furthermore, Trail et al. (2011) observe a range in fO_2 spanning 12 log units, whereas using an identical data set, the range calculated in this study is only ∼2 log units, assuming a uniform parental melt composition. The lower precision in this earlier study may be the outcome of inaccuracies involved in the estimation of $(Ce/Ce^*)_D$, since this parameter is sensitive to the concentration of LREE in zircon, and hence prone to underestimation if a LREE-bearing contaminant contributes to the zircon analysis. Moreover, it is possible that the experiments used to calibrate $(Ce/Ce^*)_D$, were subject to the same disequilibrium effects as documented by Luo and Ayers (2009), as D_{zircon} for the LREE are similar between the two studies, and larger than the measurements of Sano et al. (2002).

The range in fO_2 calculated here for Hadean zircons is strikingly similar to that of Archean komatiite (FMQ −1.5 to +1.5; Canil, 1997) and basalts (FMQ −1 to 0; Li and Lee, 2004) as well as cratonic peridotites (FMQ −1.5 to 0; Canil, 2002) as determined by vanadium partitioning. Although the currently favored model for the formation of at least the majority of these zircons is through subduction and re-melting of hydrated mafic crust, Trail et al. (2011) note that a small subset of the Hadean zircons have oxygen isotopic compositions within the mantle range. We observe no correlation between fO_2 and the oxygen isotopic composition, suggesting that interaction with the surface environment did not alter the redox state of early basaltic crust. The similarity between the crustal and mantle derived zircons is not necessarily surprising, as the mantle and surface would be close to redox equilibrium in the Hadean, as appreciable oxidation of the surface environment would not occur until much later (Farquhar et al., 2000). These results suggest that the inception of relatively oxidizing conditions in the Earth's mantle was within the first 150 Ma of the Earth's history. This is consistent with the recent suggestion that Earth accreted from oxidized material (Siebert et al., 2013), or alternatively that Earth's mantle was reduced (Wood et al., 2006) but became more oxidized through either the arrival of oxidized material during accretion (O'Neill, 1991; Siebert et al., 2013), the loss of H_2 immediately after core formation (Bali et al., 2013), or by self oxidation following accumulation of Fe^{3+} and loss of Fe^0 by disproportionation during perovskite crystallization in an early magma ocean (Wade and Wood, 2005).

7. Summary and conclusions

Using a recently developed model for the redox behavior of Ce in silicate melts, combined with lattice strain constraints on $D^{zircon/melt}_{Ce^{3+}}$ and $D^{zircon/melt}_{Ce^{4+}}$, we present a method for calculating the fO_2 at the time of crystallization from Ce anomalies in zircon. Oxygen fugacities calculated using this method typically agree with independent estimates within one log unit or better for Bishop tuff, Toba tuff and Umiakovik pluton, demonstrating that zircon can be an accurate tool in the evaluation of magma redox states. Application of this method to the Hadean zircons from the Jack Hills, Australia, result in fO_2 estimates between FMQ −1.0 and +2.5, indicating that the Earth's mantle reached its current redox state by ∼4.4 Ga.

Acknowledgements

We would like to thank Michael Bickle for editorial handling as well as Andrew Berry and Dante Canil for their thoughtful reviews. We would also like to thank John Hanchar, James Mungall, Mike Hamilton and Grant Henderson for their comments on a previous version of this manuscript. John Hanchar and Nurcahyo Basuki kindly supplied samples of the Bishop Tuff and Toba Tuff, respectively. Funding for this work was provided by NSERC Equipment, Discovery and Discovery Accelerator grants to JMB and a Geological Society of America Lipman Research Award to DJS.

Appendix A. Supplementary material

Supplementary material related to this article can be found online at http://dx.doi.org/10.1016/j.epsl.2016.08.013.

References

Anderson, A.T., Newman, S., Williams, S.N., Druitt, T.H., Skirius, C., Stolper, E., 1989. H_2O, CO_2, Cl, and gas in Plinian and ash-flow Bishop rhyolite. Geology 17, 221–225.
Bali, E., Audetat, A., Keppler, H., 2013. Water and hydrogen are immiscible in Earth's mantle. Nature 495, 220–222.
Ballard, J.R., Palin, M.J., Campbell, I.H., 2002. Relative oxidation states of magmas inferred from Ce(IV)/Ce(III) in zircon: application to porphyry copper deposits of northern Chile. Contrib. Mineral. Petrol. 144, 347–364.
Blundy, J.D., Wood, B.J., 1994. Prediction of crystal-melt partition coefficients from elastic moduli. Nature 372, 452–454.
Burnham, A.D., Berry, A.J., 2012. An experimental study of trace element partitioning between zircon and melt as a function of oxygen fugacity. Geochim. Cosmochim. Acta 95, 196–212.
Burnham, A.D., Berry, A.J., 2014. The effect of oxygen fugacity, melt composition, temperature and pressure on the oxidation state of cerium in silicate melts. Chem. Geol. 366, 52–60.
Canil, D., 1997. Vanadium partitioning and the oxidation state of Archaean komatiite magmas. Nature 389, 842–845.
Canil, D., 2002. Vanadium in peridotites, mantle redox and tectonic environments: Archean to present. Earth Planet. Sci. Lett. 195, 75–90.
Carley, T.L., Miller, C.F., Wooden, J.L., Padilla, A.J., Schmitt, A.K., Economos, R.C., Bindeman, I.N., Jordan, B.T., 2014. Iceland is not a magmatic analog for the Hadean: evidence from the zircon record. Earth Planet. Sci. Lett. 405, 85–97.
Carmichael, I.S.E., 1991. The redox states of basic and silicic magmas: a reflection of their source regions? Contrib. Mineral. Petrol. 106, 129–141.
Cavosie, A.J., Valley, J.W., Wilde, S.A., 2006. Correlated microanalysis of zircon: trace element, $\delta^{18}O$, and U–Th–Pb isotopic constraints on the igneous origin of complex >3900 Ma detrital grains. Geochim. Cosmochim. Acta 70, 5601–5616.

Cherniak, D.J., Hanchar, J.M., Watson, E.B., 1997a. Diffusion of tetravalent cations in zircon. Contrib. Mineral. Petrol. 127, 383–390.

Cherniak, D.J., Hanchar, J.M., Watson, E.B., 1997b. Rare-earth diffusion in zircon. Chem. Geol. 134, 289–301.

Chesner, C.A., 1998. Petrogenesis of the Toba tuffs, Sumatra, Indonesia. J. Petrol. 39, 397–438.

Chesner, C.A., Luhr, J.F., 2010. A melt inclusion study of the Toba Tuffs, Sumatra, Indonesia. J. Volcanol. Geotherm. Res. 197, 259–278.

Claiborne, L.L., Miller, C.F., Flanagan, D.M., Clynne, M.A., Wooden, J.L., 2010. Zircon reveals protracted magma storage and recycling beneath Mount St. Helens. Geology 38, 1011–1014.

Emslie, R.F., Loveridge, W.D., 1992. Fluorite-bearing early and middle Proterozoic granites, Okak Bay area, Labrador: geochronology, geochemistry and petrogenesis. Lithos 28, 87–109.

Emslie, R.F., Stirling, J.A.R., 1993. Rapakivi and related granitoids of the Nain plutonic suite: geochemistry, mineral assemblages and fluid equilibria. Can. Mineral. 31, 821–847.

Farquhar, J., Bao, H., Thiemens, M., 2000. Atmospheric influence of Earth's earliest sulfur cycle. Science 289, 756–758.

Ferry, J.M., Watson, E.B., 2007. New thermodynamic models and revised calibrations for the Ti-in-zircon and Zr-in-rutile thermometers. Contrib. Mineral. Petrol. 154, 429–437.

Fu, B., Page, F.Z., Cavoise, A.J., Fournelle, J., Kita, N.T., Lackey, J.S., Wilde, S.A., Valley, J.W., 2008. Ti-in-zircon thermometry: applications and limitations. Contrib. Mineral. Petrol. 156, 197–215.

Fujimaki, H., 1986. Partition coefficients of Hf, Zr, and REE between zircon, apatite, and liquid. Contrib. Mineral. Petrol. 94, 42–45.

Hanchar, J.M., van Westrenen, W., 2007. Rare earth element behavior in zircon-melt systems. Elements 3, 37–42.

Hayden, L.A., Watson, E.B., 2007. Rutile saturation in hydrous siliceous melts and its bearing on Ti-thermometry of quartz and zircon. Earth Planet. Sci. Lett. 258, 561–568.

Hildreth, W., Wilson, C.J.N., 2007. Compositional zoning of the Bishop Tuff. J. Petrol. 48, 951–999.

Hinton, R.W., Upton, B.G.J., 1991. The chemistry of zircon: variations within and between large crystals from syenite and alkali basalt xenoliths. Geochim. Cosmochim. Acta 55, 287–3302.

Hoskin, P.W.O., 2005. Trace-element compositions of hydrothermal zircon and the alteration of Hadean zircon from the Jack Hill, Australia. Geochim. Cosmochim. Acta 69, 637–648.

Hoskin, P.W.O., Schaltegger, U., 2003. The composition of zircon and igneous and metamorphic petrogenesis. Rev. Mineral. Geochem. 53, 27–62.

Li, Z.-X.A., Lee, C.-T.A., 2004. The constancy of upper mantle fO_2 through time inferred from V/Sc ratios in basalts. Earth Planet. Sci. Lett. 228, 483–493.

Luo, Y., Ayers, J.C., 2009. Experimental measurements of zircon/melt trace-element partition coefficients. Geochim. Cosmochim. Acta 73, 3656–3679.

Maas, R., Kinny, P.D., Williams, I.S., Froude, D.D., Compston, W., 1992. The Earth's oldest known crust: a geochronological and geochemical study of 3900–4200 Ma old detrital zircons from Mt. Narryer and Jack Hills, Western Australia. Geochim. Cosmochim. Acta 56, 1281–1300.

Martin, H., 1995. The Archaean grey gneisses and the genesis of the continental crust. In: Condie, K.C. (Ed.), The Archaean Crustal Evolution. Elsevier, pp. 205–259.

McDonough, W.F., Sun, S.-s., 1995. The composition of the Earth. Chem. Geol. 120, 223–253.

Nagasawa, H., 1970. Rare earth concentrations in zircons and apatites and their host dacites and granites. Earth Planet. Sci. Lett. 9, 359–364.

O'Neill, H.St.C., 1987. Quartz–fayalite–iron and quartz–fayalite–magnetite equilibria and the free energy of formation of fayalite (Fe_2SiO_4) and magnetite (Fe_3O_4). Am. Mineral. 72, 67–75.

O'Neill, H.St.C., 1988. Systems Fe–O and Cu–O: thermodynamic data for the equilibria Fe–"FeO," Fe–Fe_3O_4, "FeO"–Fe_3O_4, Fe_3O_4–Fe_2O_3, Cu–Cu_2O, and Cu_2O–CuO from emf measurements. Am. Mineral. 73, 470–486.

O'Neill, H.St.C., 1991. The origin of the Moon and the early history of the Earth—a chemical model. Part 2: the Earth. Geochim. Cosmochim. Acta 55, 1159–1172.

Reid, M.R., Vazquez, J.A., Schmitt, A.K., 2011. Zircon-scale insights into the history of a Supervolcano, Bishop Tuff, Long Valley, California, with implications for the Ti-in-zircon geothermometer. Contrib. Mineral. Petrol. 161, 293–311.

Rudnick, R.L., Gao, S., 2003. Composition of the continental crust. In: Heinrich, D.H., Karl, K.T. (Eds.), Treatise on Geochemistry. Pergamon, Oxford, pp. 1–64.

Sano, Y., Terada, K., Fukuoka, T., 2002. High mass resolution ion microprobe analysis of rare earth elements in silicate glass, apatite and zircon: lack of matrix dependency. Chem. Geol. 184, 217–230.

Shannon, R.D., 1976. Revised effective ionic radii and systematic studies of interatomic distances in halides and chaleogenides. Acta Crystallogr., Sect. B Struct. Sci. 32, 751–767.

Siebert, J., Badro, J., Antonangeli, D., Ryerson, F.J., 2013. Terrestrial accretion under oxidizing conditions. Science 339, 1194–1197.

Smythe, D.J., Brenan, J.M., 2015. Cerium oxidation state in silicate melts: combined fO_2, temperature and compositional effects. Geochim. Cosmochim. Acta 170, 173–187.

Thomas, J.B., Bodnar, R.J., Shimizu, N., Sinha, A.K., 2002. Determination of zircon/melt trace element partition coefficients from SIMS analysis of melt inclusions in zircon. Geochim. Cosmochim. Acta 66, 2887–2901.

Trachenko, K., Dove, M.T., Salje, E.K.H., 2002. Structural changes in zircon under alpha-decay irradiation. Phys. Rev. B 65, 180102(R).

Trail, D., Watson, E.B., Tailby, N.D., 2011. The oxidation state of Hadean magmas and implications for early Earth's atmosphere. Nature 480, 79–82.

Trail, D., Watson, E.B., Tailby, N.D., 2012. Ce and Eu anomalies in zircon as proxies for the oxidation state of magmas. Geochim. Cosmochim. Acta 97, 70–87.

Virgo, D., Mysen, B.O., Kushiro, I., 1980. Anionic constitution of 1-atmosphere silicate melts: implications for the structure of igneous melts. Science 20, 1371–1373.

Wade, J., Wood, B.J., 2005. Core formation and the oxidation state of the Earth. Earth Planet. Sci. Lett. 236, 78–95.

Wallace, P.J., Anderson, A.T., Davis, A.M., 1999. Gradients in H_2O, CO_2, and exsolved gas in a large-volume silicic magma system: interpreting the record preserved in melt inclusions from the Bishop Tuff. J. Geophys. Res., Solid Earth 104, 20097–20122.

Watson, E.B., Harrison, T.M., 1983. Zircon saturation revisited: temperature and composition effects in a variety of crustal magma types. Earth Planet. Sci. Lett. 64, 295–304.

Watson, E.B., Harrison, T.M., 2005. Zircon thermometer reveals minimum melting conditions on earliest Earth. Science 308, 841–844.

Wilde, S.A., Valley, J.W., Peck, W.H., Graham, C.M., 2001. Evidence from detrital zircons for the existence of continental crust and oceans on the Earth 4.4 Gyr ago. Nature 409, 175–178.

Wilson, C.J.N., Hildreth, W., 1997. The Bishop Tuff, new insights from eruptive stratigraphy. J. Geol. 105, 407–439.

Wood, B.J., Walter, M.J., Wade, J., 2006. Accretion of the Earth and segregation of its core. Nature 441, 825–833.